Spectrochimica Acta Part A: Molecular and Biomolecular Spectroscopy 139 (2015) 321–328

Contents lists available at ScienceDirect

Spectrochimica Acta Part A: Molecular and Biomolecular Spectroscopy

journal homepage: www.elsevier.com/locate/saa

Conformational analysis, X-ray crystallographic, FT-IR, FT-Raman, DFT, MEP and molecular docking studies on 1-(1-(3-methoxyphenyl) ethylidene) thiosemicarbazide

R.R. Saravanan [a,*], S. Seshadri [b], S. Gunasekaran [c], R. Mendoza-Meroño [d], S. Garcia-Granda [d]

[a] Department of Physics, Misrimal Navajee Munoth Jain Engineering College, Thoraipakkam, Chennai 600 097, India
[b] Department of Physics, L.N. Govt. Arts College, Ponneri, Thiruvallur 601 001, India
[c] Research & Development, St. Peter's University, Avadi, Chennai 600 054, India
[d] Faculty of Chemistry, Department of Physical and Analytical Chemistry, University Oviedo, C/ Julian Claveria, 8, 33006 Oviedo, Asturias, Spain

HIGHLIGHTS

- The FT-IR, FT-Raman studies were carried out for synthesized MPET.
- MEP plays an important role in determining the stability of the MPET.
- Structures of MPET have been studied by spectroscopic and X-ray diffraction method.
- Conformational analysis used to examine the positions of a MPET molecule.

GRAPHICAL ABSTRACT

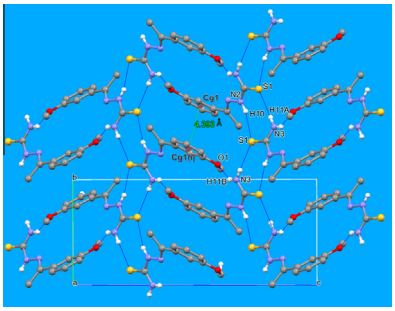

ARTICLE INFO

Article history:
Received 23 July 2014
Received in revised form 22 November 2014
Accepted 10 December 2014
Available online 30 December 2014

Keywords:
MPET
FT-IR
FT-Raman
Docking
Crystallography

ABSTRACT

Conformational analysis, X-ray crystallographic, FT-IR, FT-Raman, DFT, MEP and molecular docking studies on 1-(1-(3-methoxyphenyl) ethylidene) thiosemicarbazide (MPET) are investigated. From conformational analysis the examination of the positions of a molecule taken and the energy changes is observed. The docking studies of the ligand MPET with target protein showed that this is a good molecule which docks well with target related to HMG-CoA. Hence MPET can be considered for developing into a potent anti-cholesterol drug. MEP assists in optimization of electrostatic interactions between the protein and the ligand. The MEP surface displays the molecular shape, size and electrostatic potential values. The optimized geometry of the compound was calculated from the DFT–B3LYP gradient calculations employing 6-31G (d, p) basis set and calculated vibrational frequencies are evaluated via comparison with experimental values.

Introduction

Thiosemicarbazones are compounds that have been studied for a considerable period of time for their biological properties. Traces of interest date back to the beginning of the 20th century, but the first reports on their medical applications began to appear in the Fifties as drugs against tuberculosis and leprosy [1,2]. Thiosemicarbazones are a class of small molecules that has been evaluated over the last 50 years as antivirals [3,4] and as anticancer therapeutics, [5] as well as for their parasiticidal action against *Plasmodium falciparum* [6] and *Trypanosoma cruzi* [7,8] which are the causative agents of malaria and Chagas's disease, respectively. Brockman et al. first showed that 2-formylpyridine thiosemicarbazone

* Corresponding author. Mobile: +91 99940 31849.
E-mail address: saravapj@gmail.com (R.R. Saravanan).

http://dx.doi.org/10.1016/j.saa.2014.12.026
1386-1425/

Table 1
Details of the experimental diffraction data collections and refinements.

	I
Empirical formula	$C_{10}H_{13}N_3OS$
Formula weight	223.29
Color, shape	Colorless
Temperature (K)	293
Crystal size (mm)	0.20 0.17 0.11
Crystal system	Monoclinic
Space group	$P2_1/c$
Lattice constants	
a (Å)	6.9460(1)
b (Å)	8.4300(2)
c (Å)	19.6150(2)
α (°)	90.00
β (°)	99.722(2)
γ (°)	90.00
Volume (Å^3)	1140.7(3)
Z	4
λ (Å)	1.5418
Calculated density, ρ (g cm^{-3})	1.300
θ rang for data collection (°)	4.53–73.03
Absorption coefficient (mm^{-1})	2.350
F(000)	472
Reflections collected	4538
Independent reflections	2201 [*R*(int) = 0.0140]
Parameters	188
Goodness-of-fit on F^2	1.061
Final *R* indices [$I > 2\sigma(I)$]	*R*1 = 0.0327
	w*R*2 = 0.0908
R indices (all data)	*R*1 = 0.0340
	w*R*2 = 0.0923
Largest Δ*F* peak and hole (e Å^{-3})	0.188 and −0.182

Table 2
Hydrogen-bond geometry (Å, °).

D–H···A	D–H (Å)	H···A (Å)	D···A (Å)	D–H···A (°)
N(2)–H(10)···S(1) (i)	0.88(2)	2.68(2)	3.526(2)	162.1(2)
N(3)–H(11a)···S(1)(ii)	0.90(2)	2.48(2)	3.344(2)	160.4(2)
N(3)–H(11b)···O(1)(iii)	0.90(2)	2.27(2)	3.071(2)	149.1(2)

Symmetry Codes (i) −*x*, 1/2+*y*, 1/2−*z* (ii) −*x*, −1/2+*y*, 1/2−*z* (iii) 1−*x*, 2−*y*, −*z*.

possesses anti-leukemic activity in mice bearing leukemic cells [9]. Following this report, various aliphatic, aromatic, and heteroaromatic carbaldehyde thiosemicarbazones were synthesized and evaluated for antitumor activity against a wide spectrum of transplanted murine neoplasms [10]. Vibrational spectroscopy has the potential to yield valuable structural and conformational information of organic compounds if used in conjugation with accurate quantum chemical calculations. [11].

During the last few years, a variety of experimental methods developed by physicists and biologists allowed direct monitoring of ligand-receptor interaction at the single molecule level. The continual progress within the field of crystallography, spectroscopy and Bioinformatics made available the structure of many ligand–receptor complexes with angstrom resolution. In this paper, we present, the conformational stability, synthesis, X-ray crystallographic, molecular structure, spectroscopic characterization and molecular docking studies of 1-(1-(3-methoxyphenyl) ethylidene) thiosemicarbazide (MPET). The optimized geometry and vibrational wavenumbers for conformers of MPET were calculated at the B3LYP level of theory with the 6-31G basis set. In order to provide templates for molecular modeling studies, experimental results obtained from X-crystallography and those from B3LYP methods were compared. The possible stable conformers of (MPET) were searched. Molecular docking studies for MPET also performed to find the interaction with anti cholesterol target.

Experimental

Sample preparation

A solution of 1-(3-methoxyphenyl) ethanone (3.003 g 0.02 mol) and thiosemicarbazide (1.82 g, 0.02 mol) in absolute methanol (80 ml) was refluxed for 2 h in the presence of p-toluenesulfonic acid as a catalyst, with continuous stirring. On cooling to room temperature the precipitate was filtered off, washed with copious cold methanol and dried in air. Colorless single crystals of MPET were obtained after recrystallization from a solution in methanol. 1H-RMN (DMSO-d6): σ (ppm) 2.28 (s 3H, CH_3) 3.806 (s 3H,

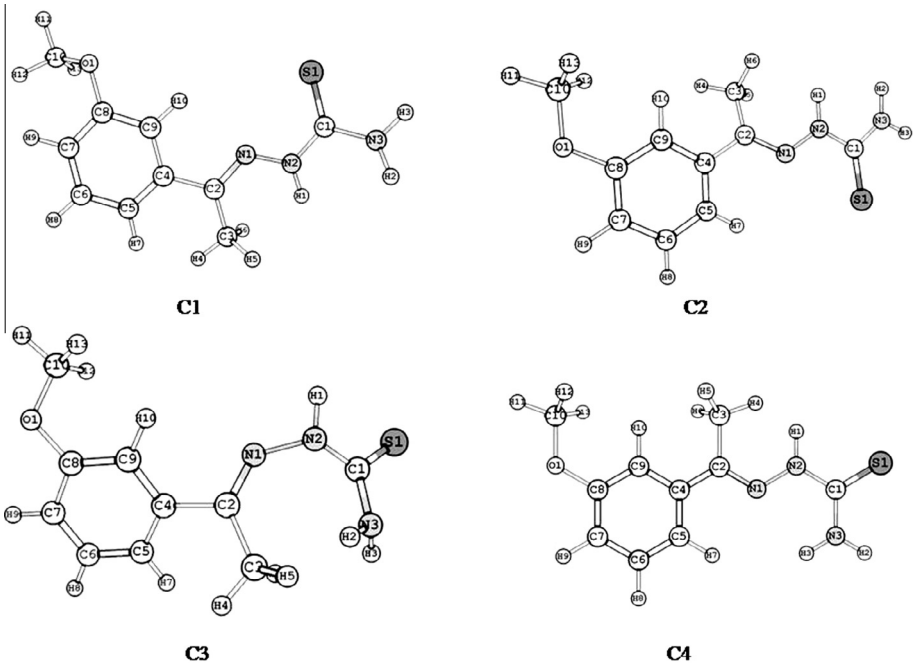

Fig. 1. The various possible stable conformers of MPET.

Table 3
Total energies of different conformations of MPET calculated at the B3LYP/6-31G (d, p) level of theory.

S. No.	Conformer	Energy (Hartree)	kJ/mol	Energy difference (kJ/mol)
1.	C2	−1026.53914423	−2695178.72848369	0.000
2.	C1	−1026.52692861	−2695146.65637094	32.072
3.	C3	−1026.49678837	−2695067.52316479	111.205
4.	C4	−1026.49440378	−2695061.26242327	117.466

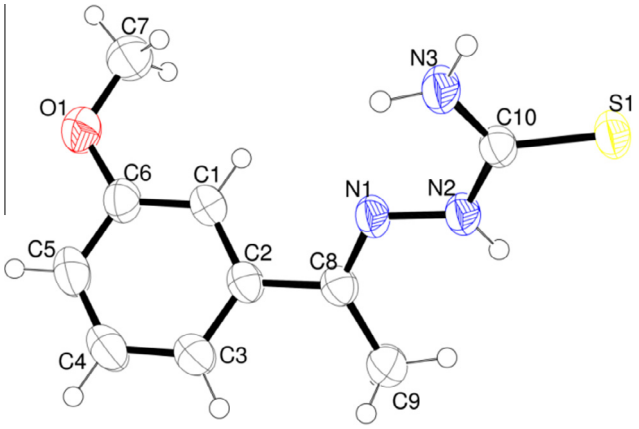

Fig. 2. The structure of the title compound showing 50% probability displacement ellipsoids and the atom-numbering scheme.

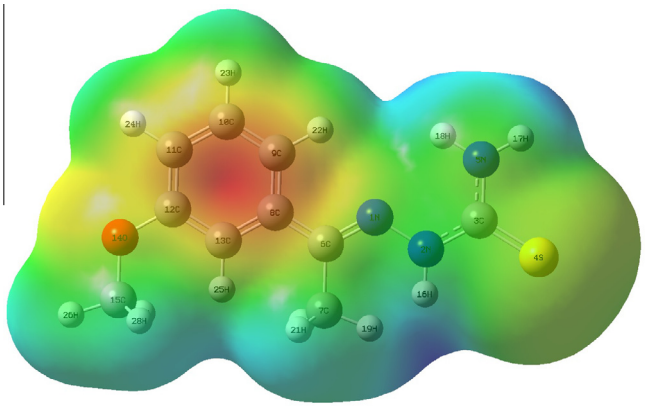

Fig. 4. MEP of MPET.

OCH_3) 6.95–6.98 (d 1H, Ar-H) 7.28–7.32 (t 1H, Ar-H) 7.44–7.47 (d 1H, Ar-H) 7.44 (s 1H, Ar-H), 7.93 (s 1H, NH_2) 8.27 (s 1H, NH_2) 10.19 (s, –CNH-N). 13C-RMN (DMSO-d_6): σ (ppm) 14.45 (1C, $-CH_3$) 55.41 (1C, $-OCH_3$) 112.05 (1C, aromatic) 115.20 (1C, aromatic) 119.36 (1C, aromatic) 129.47 (1C, aromatic) 139.36 (1C, aromatic) 147.95 (1C, aromatic) 159.55 (1C, –C═N) 179.12 (1C, C═S).

Single crystal X-ray structure determination

The diffraction data from a selected single crystal was collected at room temperature on Oxford Diffraction Xcalibur Gemini S diffractometer equipped with CuKα radiation (λ = 1.5418 Å). The data were processed with CrysAlis software and Empirical absorption correction using spherical harmonics, were implemented with SCALE3 ABSPACK scaling algorithm [12]. The crystallographic data, the data collection parameters, and the refinement parameters for each structure are summarized in Table 1. The Hydrogen Bond geometry of MPET is given in Table 2.

Crystal structure was solved by direct methods using Sir2008 [13] and refined by full-matrix least-square calculations against F^2 using SHELXL [14]. All non-hydrogen atoms were refined with anisotropic displacement parameters. All the hydrogen atoms were located at the difference Fourier map in isotropically refined. The

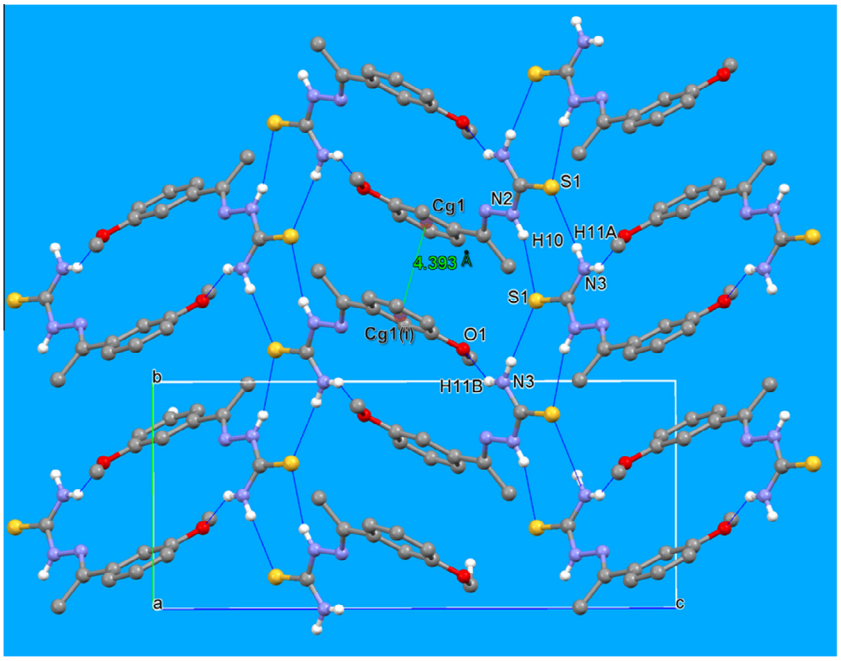

Fig. 3. Intermolecular interactions in the crystal packing along *bc* plane.

figures were produced using ORTEP-3 [15] MERCURY [16]. The software used for the preparation of the materials for publication: WinGX [17], PLATON [18], PARST [19].

Computational method

The combination of spectroscopic methods with DFT calculations are powerful tools for understanding the fundamental vibrational properties and the electronic structure of the compounds [20]. The entire calculations carried out in the present work were performed at B3LYP levels included in the Gaussian 03W [21] package program with the 6-31G (d, p) basis set functions of the DFT utilizing gradient geometry optimization [22]. All the geometries were optimized using the 6-31G (d, p) basis set using DFT [23] employing Becke's three parameter hybrid functional [24] combined with the Lee–Yang–Parr correlation [25] functional (B3LYP) method. By combining the results of the Gaussview program [26] with symmetry considerations, vibrational band assignments were made with a high degree of accuracy. In order to find the most optimized geometry, the energy calculations were carried out using the B3LYP method with 6-31G (d, p) basis set for 4 different possible conformers.

Results and discussion

Conformational analysis

Conformational analysis is the examination of the positions a molecule takes and the energy changes it undergoes as it converts among its different conformations. Because each of the various conformations of a molecule has different properties, the conformation the molecule normally adopts has a deep influence on its physical and chemical properties. The various possible stable conformers of MPET were shown in Fig. 1. From B3LYP/6-31G (d, p) calculation the conformer C2 is predicted more stable from 32.072 to 117. 466 kJ/mol than the other MPET conformers. When comparing C2 with C4 the positional change of atoms like S and NH_2. This change makes the structure C2 has more energy than C4. When comparing C3 and C4 the orientation of both CH_3 and NH_2 group are changed, but this makes very small change in the energy. The total energies obtained for these conformers were shown in Table 3. It is clear from Table 3 that the conformer C2 has produced the global energy minimum.

X-ray of the crystal structures

The compound crystallizes in the monoclinic lattice with $P2_1/c$ symmetry. The ORTEP diagram of MPET is shown in Fig 2, displacement ellipsoids are drawn at 50% probability level. The molecular conformation in the crystal the C9–C8/N1/N2/S1 plane form a dihedral angle of 42.73 (5)° with the benzene ring (C1–C6). The C═N bond length [1.280 (2) Å] and C═S bond length [1.6916 (2) Å] are in agreement with those values observed before (Wang et al. [27]).

The crystal packing is established by typical intermolecular N–H···S hydrogen-bond interactions of thiosemicarbazone moiety, forming sheets along the *2₁ axes*. The methoxy group is involved in N–H···O strong hydrogen bond *Fig 3*. Additionally π–π stacking interactions [Cg1 (C1→C6)···Cg1 (iv) = 4.3934 (2) Å, offset = 25.52° for [iv: 1−*x*, 1−*y*, −*z*] are present in the crystal contributing to stabilize chains. The Details of the experimental diffraction data collections and refinements are shown in Table 1.

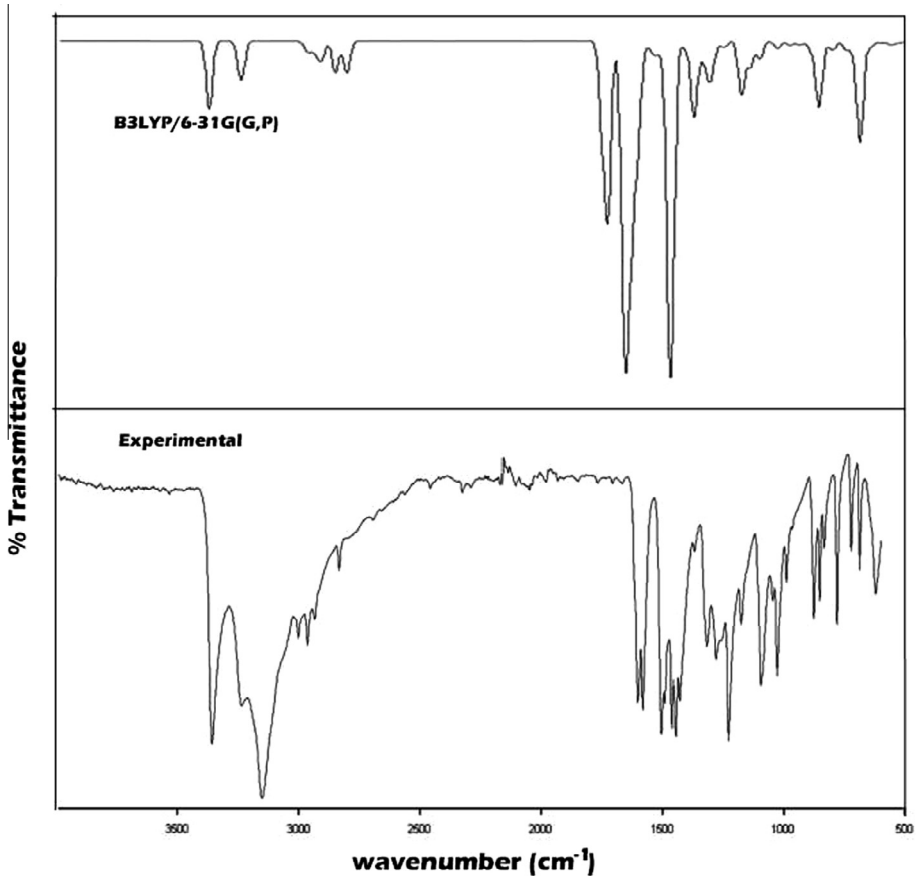

Fig. 5. Theoretical and experimental FT-IR spectra of MPET.

Molecular electrostatic potential (MEP)

Molecular electrostatic potential (MEP) mapping is very useful in the investigation of the molecular structure with its physiochemical property relationships [28–31]. Molecular electrostatic potential surfaces are important in computer-aided drug design as a result of them assisting in optimization of electrostatic interactions between the protein and the ligand. These surfaces are accustomed compare different inhibitors with substrates or transition states of the reaction. Electrostatic potential surfaces are either displayed as isocontour surfaces or mapped onto the molecular electron density. The later are more widely used because they maintain the sense of underlying chemical structure better than isocontour plots. The MEP surface displays the molecular shape, size and electrostatic potential values. The color scheme for the MEP surface is partially negative charge or red-electron rich; partially positive charge or blue-electron deficient; yellow-slightly electron rich region; light blue-slightly electron deficient region, respectively. Potential increases in the order red < orange < yellow < green < blue. The MEP diagram of MPET is shown in Fig. 4. The MPET molecule must present atoms either with positive potential isosurface and atoms with negative potential isosurface. The MEP of MPET clearly indicates the electron rich centers of sulfur and the positive potential isosurface centers of N1, O1 and H11B.

Vibrational assignments

N–H vibrations

The N-H stretching vibrations give rise to a weak band at 3500–3300 cm^{-1}. Saravanan et al. [32] have observed the N–H stretching band at 3393 cm^{-1} in FT-IR and 3395 cm^{-1} in FT Raman spectra of (E) -1-[1-(4-Chlorophenyl) ethylidene] thiosemicarbazide). In the experimental FTIR spectrum of MPET observed at 3441, 3455 cm^{-1} and in FT Raman 3445, 3453 cm^{-1} is assigned to symmetric N–H stretching vibration with PEDs 99% and 99% respectively. The symmetric stretching mode calculated at 3443, 3456 cm^{-1} by B3LYP/6-31G (d, p). Fig. 5 shows that the comparison of theoretical and experimental FT-IR spectra of MPET. Fig. 6 shows that the comparison of theoretical and experimental FT-Raman spectra of MPET.

C–H vibrations

The C–H stretching vibrations of aromatic and hetero aromatic structures occur [33,34] in the region 3100–2900 cm^{-1} for asymmetric stretching modes of vibrations. This permits the ready identification of the structure. A medium band is observed at 2916 and 2962 cm^{-1} in infrared and an intense band is observed at 2920 and 2961 cm^{-1} in FT-Raman can be assigned to C–H stretching respectively. The corresponding calculated fundamentals using B3LYP/6-31G (d, p) are 2919 and 2962. The theoretically scaled vibrations

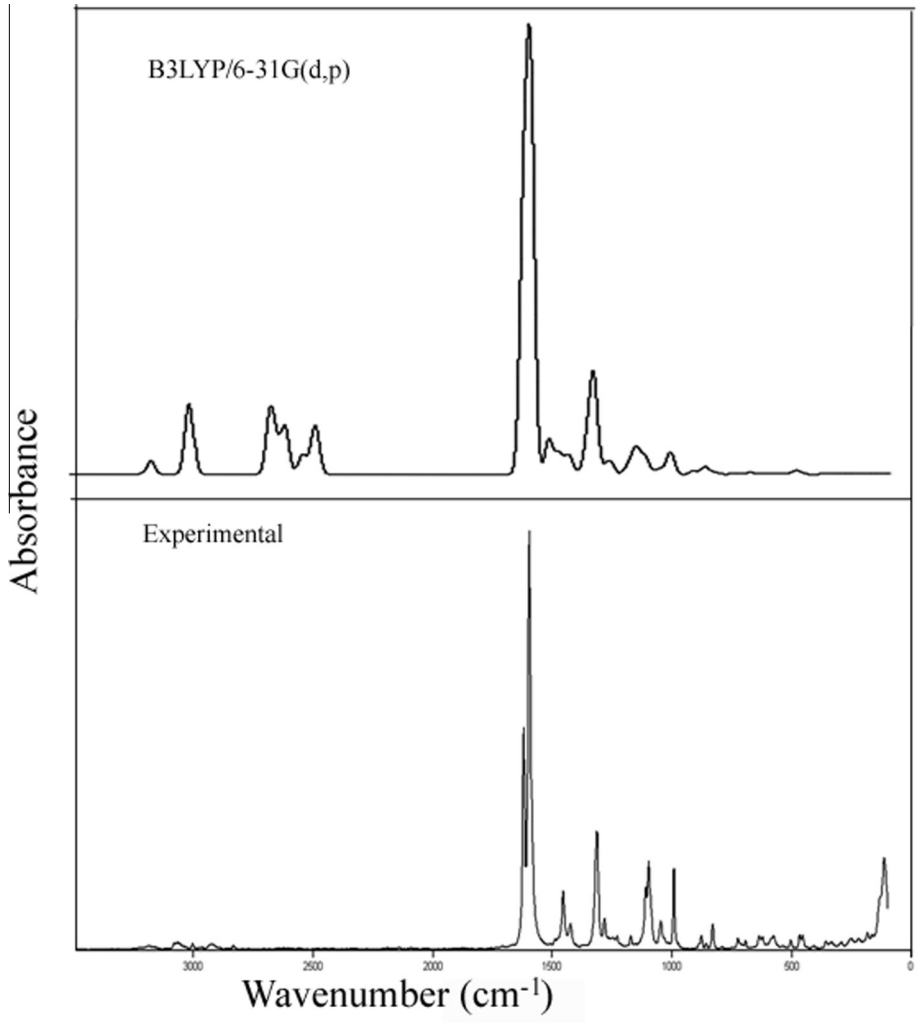

Fig. 6. Theoretical and experimental FT-Raman spectra of MPET.

Table 4
Theoretical and experimental vibrational wavenumbers (cm^{-1}) of MPET Calculated using B3LYP/6-31G (d, p).

ν_{IR} cm^{-1}	ν_{Raman} cm^{-1}	ν_{cal} cm^{-1}	IR intensity	Raman activity	*P*	Reduced mass	Force constant	Characterisation of normal modes with PED (%)
		26	4.3542	3.7119	0.6085	4.3542	0.0021	τ ring (11) + CH_3 twist (17)
		39	7.5068	2.7877	0.7386	7.5068	0.0077	τ ring (16) + τCN(27)
		64	5.9822	1.6427	0.7007	5.9822	0.0163	τ CH_3(18) + γCH(18)
		87	1.7265	0.7491	0.7207	3.2956	0.0163	τCH_3(21)
		101	3.9113	4.9905	0.4538	4.0950	0.0268	γ CH_3(33) + τCN(25)
	115	120	0.2783	1.6370	0.7499	2.1853	0.0203	γ CH_3(26)
		144	2.3858	2.2641	0.6963	2.4891	0.0332	CN_{rock} (41)
	166	168	0.7045	2.3952	0.3824	2.1176	0.0385	CN_{rock} (36)
		204	7.7305	4.0996	0.4758	3.4792	0.0924	τCH_3(33)
	216	212	2.3260	2.8639	0.7245	2.1867	0.0619	τCH_3(24) + γCS (15)
	251	256	149.7140	1.4301	0.6685	1.3275	0.0557	γNH_2(43) + γCN (13)
		267	12.3150	3.4716	0.4698	1.6434	0.0749	τCH_3(27)
	294	286	19.1545	0.5755	0.4659	3.4617	0.1802	τ ring (18)
		315	4.9603	2.4979	0.2448	2.9495	0.1875	β CH_3(23)
	336	333	10.7059	0.8660	0.4019	4.4755	0.3164	β CCH(21) + δCS (16)
	405	400	14.4834	3.2431	0.2886	5.3126	0.5379	β NCS (26)
		421	1.3401	12.9384	0.4935	3.7885	0.4291	β NH_2 (31) + νCH (59)
		441	4.5653	3.9710	0.3992	3.5444	0.4390	β ring (37) + νCN (65)
	451	449	0.3528	4.0438	0.1939	4.0951	0.5191	β ring (32)
	469	470	104.6209	1.1166	0.7472	1.2058	0.1702	γ NH(27)
	504	505	13.8440	4.3139	0.2082	4.5765	0.7450	β CCC (16)
	533	528	3.1115	2.5292	0.2854	4.0873	0.7246	ωCH (15) + CH_{3scis}(16)
		560	2.6713	3.0754	0.4978	4.2962	0.8590	β ring (26) + νCO (54)
	577	574	3.8228	0.0970	0.5923	1.4837	0.3120	τNH_2 (22) + νCO (61)
		610	0.3992	0.6858	0.6703	4.0140	0.9515	Ring breathing (65)
622	622	619	4.7611	4.4126	0.7027	4.0441	0.9875	β ring (24) + γCO (45)
	633	628	1.4329	6.3711	0.7316	2.5420	0.6372	β CNH (31) + νCS (69)
681	678	679	9.3106	2.0878	0.7207	2.2721	0.6686	CH_3opr (18) + γ CH (26)
	695	697	3.1283	7.2100	0.5439	4.8040	1.4942	β CCH (15) + νCN (72)
778		775	28.1163	9.7691	0.3567	1.4230	0.5430	γCH (15) + γCO (26)
		818	21.0770	31.7347	0.1791	3.1864	1.3579	γCN (29) + β CNH (15)
833	830	832	23.7718	1.8974	0.3551	1.5522	0.6835	γCH twist (19) + δCO (23)
860	862	865	52.5218	13.9415	0.3309	2.4989	1.2026	β ring (21) + δCH_3 (17)
877	878	875	35.2894	2.7519	0.6868	1.7832	0.8690	τCH(43)+δCH_3 (21)
	946	943	0.6533	1.8875	0.4316	1.2711	0.7203	δCH_3 (46) + δCH(35)
965		962	9.1096	18.4484	0.2247	2.3212	1.3654	β CCH(67)
	974	973	1.0961	78.5506	0.1540	5.8763	3.5419	δCH_3 (27) + δCH(14)
	997	1001	1.5534	8.8515	0.4223	1.5819	1.0195	δCH_3 (24)+δCH(32)
	1015	1017	21.7532	14.9224	0.5589	2.2583	1.4889	β CCC(15)
1031	1032	1035	52.0104	3.2886	0.4833	4.4959	3.0847	γCC (16) + τCH_3(26)
		1066	17.2099	22.7360	0.2681	1.8048	1.3031	CH_3opr (78) + δCH(31)
1086		1082	9.9143	61.6583	0.2496	1.6818	1.2527	β CCH(32)
	1110	1114	120.3939	103.0271	0.3343	4.1043	3.2479	CH_3opr(20) + γCC (51)
		1134	0.6475	4.3457	0.7485	1.2732	1.0413	CH_3opr (45) + γCC (32)
1151	1152	1148	8.1783	39.0904	0.3394	1.1265	0.9387	CHipr (56) + νNN(77)
1173	1171	1169	7.8691	8.3031	0.5794	1.3929	1.2067	δCH_3 (63) + δCH (29)
1229	1229	1225	200.1657	41.2047	0.4438	2.6359	2.5173	δCH_3 (28)+ β CCH (79)
	1244	1243	418.7783	24.5974	0.3748	1.9619	1.9295	δCH (47) + δCC(64)
1282	1281	1279	12.9725	14.8739	0.5408	2.0929	2.1634	δCH_3 (13) + νCN (69)
		1297	11.4490	388.3666	0.3125	2.9000	3.1013	δCC (31) + νCN (56)
1319	1318	1321	19.2909	152.4666	0.2578	3.8786	4.3231	γCH_3 (10) + δCC (73)
1364	1362	1363	7.7079	9.7992	0.7496	1.2737	1.5056	νCC (81)
	1403	1405	123.2757	70.4237	0.3001	2.5009	3.1408	γCH_3 (19)+ δCH(13)
		1406	14.0800	8.6845	0.1621	2.3578	2.9671	β CH_3(21)+υCO (79)
1429	1427	1432	189.7236	14.7229	0.5921	1.2106	1.5824	νCN (84)
		1439	3.8316	18.1702	0.1993	1.3957	1.8401	CH_3scis (61) + δCH (37)
1446		1448	7.3721	27.0013	0.7500	1.0471	1.3969	CH_3scis (46) + νCN (82)
	1455	1452	75.2736	19.3178	0.5390	1.1270	1.5115	β CH_3(31)
1463		1460	142.2858	16.1730	0.7107	1.1273	1.5296	νCN (78) + δCH(65)
	1478	1474	335.7285	10.4048	0.3175	1.6377	2.2642	νCN (62) + δCH (26)
1492	1489	1490	62.9492	136.8894	0.3984	1.9879	2.8070	νCH (45) + νCC(23)
		1561	263.4853	183.0268	0.3402	1.6242	2.5149	νCC(63)
		1568	7.2270	1381.9847	0.3380	5.8616	9.1719	δ CH_3 (11) + νCN (60)
1589	1592	1590	121.9896	534.3458	0.3885	5.4348	8.7486	νCO (89)
1604		1603	5.9833	702.2122	0.2999	8.8243	14.4293	νC=N (96)
		2902	46.4998	123.2235	0.0289	1.0351	5.5424	νC–H (98)
2916	2920	2919	7.2530	111.8711	0.0069	1.0429	5.6501	νC–H(99)
2962	2961	2962	41.0482	40.6345	0.7498	1.1061	6.1678	νC–H(99)
	2970	2968	9.9206	46.0600	0.7499	1.1006	6.1650	νC–H(99)
	3038	3034	27.9342	173.7227	0.4475	1.0996	6.4352	$\nu_s CH_3$(98)
	3053	3051	7.6161	39.1178	0.5383	1.0950	6.4813	$\nu_s CH_3$(99)
	3063	3071	11.7149	90.0515	0.5080	1.0880	6.5262	νCH_3(98)
	3100	3097	6.3808	169.4561	0.2942	1.0930	6.6628	$\nu_a CH_3$(100)
	3102	3107	5.9265	67.6353	0.1166	1.0931	6.7086	$\nu_a CH_3$(98)

Table 4 (*continued*)

ν_{IR} cm^{-1}	ν_{Raman} cm^{-1}	ν_{cal} cm^{-1}	IR intensity	Raman activity	*P*	Reduced mass	Force constant	Characterisation of normal modes with PED (%)
	3111	3111	5.6715	52.1374	0.2443	1.0888	6.7000	νC–H(100)
3441	3445	3443	32.7024	189.4240	0.2148	1.0754	8.1026	νNH(99)
3455	3453	3456	36.0834	128.9123	0.1223	1.0477	7.9536	$\nu_s NH_2$(99)
3620	3617	3615	109.2166	58.0800	0.6396	1.1036	9.1679	$\nu_a NH_2$(98)

ν: stretching; β: in-plane bending; γ: out-of-plane bending; asym: asymmetric stretching; sym: symmetric stretching; ipr: in-plane rocking; opr: out-of-plane rocking; τRing: ring out of-plane bending; scis: scissoring; wag: wagging.

by B3LYP/6-31G (d, p) level method also show good agreement with experiment recorded data.

The bands due to C–H in-plane bending vibrations are observed in the region 1000–1300 cm^{-1} [35]. In the present study the C–H in plane bending vibrations were observed at 1173 and 1229 cm^{-1} in FT-IR and at 1171 and 1229 cm^{-1} in FT-Raman. The deviation is 2 cm^{-1} between experimental and calculated B3LYP/6-311++G (d, p) values in MPET show better agreement with theoretical values. The C–H out-of-plane bending vibrations appear within the region 900–675 cm^{-1} [36]. The vibrations identified at 681 cm^{-1} in FT-IR and 678 cm^{-1} in FT-Raman are assigned to C–H out-of-plane bending for MPET. The B3LYP level at 6–31G (d, p) gives the wavenumber value at 679 cm^{-1} for C–H out-of-plane bending and are shown in Table 4.

C–C vibrations

The C–C stretching modes of the phenyl group are expected in the range from 1650 to 1200 cm^{-1}. The actual position of these modes is determined not to much by the nature of the substituent's but by the form of substitution around the ring [37]. In the present study, the bands at 1492 and 1364 cm^{-1} in FT-IR spectrum and 1489 and 1362 cm^{-1} in FT-Raman are assigned to C-C stretching vibration for our MPET molecule. The theoretically computed wavenumbers at 1490 and 1363 cm^{-1} in B3LYP method also correlated with the experimental observations. The calculated PED values corresponding to these two modes are 23% and 81%.

C–N vibrations

Saravanan et al. [32] have observed the C–N stretching band at 1296 cm^{-1} in FT-IR and 1291 cm^{-1} in FT-Raman spectrum of (E) -1-[1-(4-Chlorophenyl) ethylidene] thiosemicarbazide. In the present work, the bands at 1282 and 1281 cm^{-1} in the FT-IR and FT-Raman spectrum of MPET are assigned to the C-N stretching mode of vibrations respectively. The calculated bands at a B3LYP level in the same region show band positions at 1279 cm^{-1} for C–N vibrations.

N–N vibrations

Azo compounds are difficult to identify by IR spectroscopy because no significant bands are observed for those, the azo group being non polar in nature [38–40]. Crane et al. [41] have observed the N-N stretching band at 1151 cm^{-1} and Seena et al. [42] at 1136 cm^{-1}. In the present work the band appears at 1151 cm^{-1} in FT-IR and 1152 cm^{-1} in FT-Raman assigned to N–N vibrations. The theoretically computed values by B3LYP/6-31G (d, p) method for N–N vibrations coincide with experimental values.

Molecular docking studies

The structure of the target receptor, Human reductase with HMG-CoA (PDB id: 1DQ8) were obtained from the RCSB protein databank [http://www.rcsb.org/pdb]. Protein retrieved from the database was analyzed for pockets before docking studies, to ensure the possible number of binding sites of protein and ligand. The binding sites for the target receptor were searched from the Q-site finder [www.bioinformatics.leeds.ac.uk/qsitefinder]. The small molecule or ligand is optimized by Gaussian 03W [21] package in the basis set B3LYP/6-31G (d, p). The ligand–protein docking simulations are carried out by Autodock tools [43] V1.5.4. and Autodock V4.2. Programs.

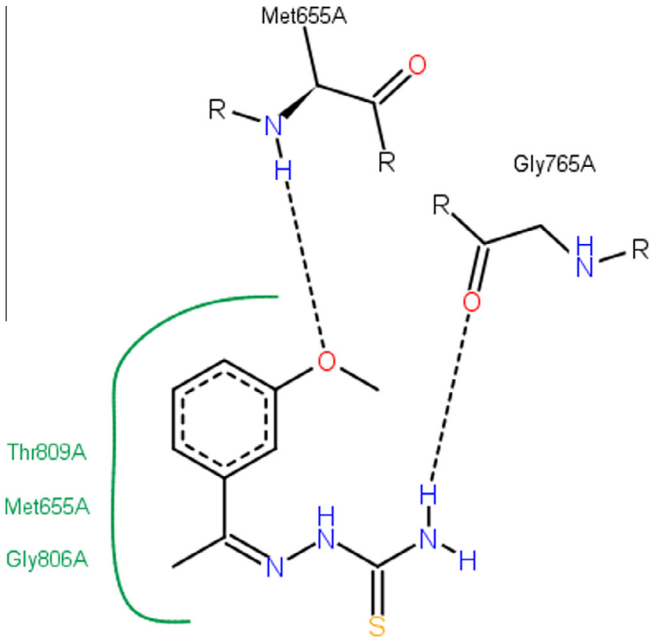

Fig. 7. Poseview of MPET with HMG-CoA receptor, dotted lines shows hydrogen bonds.

The non bonded atoms in the target receptor like an oxygen atom of H_2O molecules that were present in the crystal structure of Human reductase with HMG and CoA, is cleaned up by removing H_2O molecules and hydrogen atoms also added. Autodock docks a flexible ligand to a rigid receptor. Affinity maps for all the atom types present as well as electrostatic map, were computed with grid spacing of 0.375 E. Evaluation of the results was done by sorting the different complexes with respect to predicted binding energy.

The Autodock V4.2 software is used to simulate the binding mode of the target receptor and ligand. The protein structure of HMG-CoA reductase (PDB ID: 1DQ8) used as a target receptor. Fig. 7 shows the poseview of MPET with HMG-CoA receptor. Poseview [44–46], a tool which displays molecular complexes incorporating a simple, easy-to-perceive arrangement of the ligand and the amino acids towards which it forms interactions. HMG-CoA reductase is the rate controlling enzyme of the mevalonate pathway, the metabolic pathway that produces cholesterol and isoprenoids. The 10 docking candidates were ranked by energy and the one with the lowest energy was regarded as the best mimic structure. There are two hydrogen bonds joining MPET and HMG-CoA reductase.

The hydrogen bonds between HMG-CoA and MPET also shown in Fig. 7. Hydrogen bonding in docking plays a significant role in interaction studies. The hydrogen bonds formed between N1, O1 and H11B with GLY806, MET655 and GLY765, the distance are 3.5, 3.1 and 2.2 Å. The energy value between binding sites of HMG-CoA and MPET are −5.08 kcal/mol.

Conclusion

The FT-IR, FT-Raman studies were carried out for synthesized MPET. DFT calculations at the B3LYP/6-31G (d, p) level of theory were performed in order to analyze structural properties of MPET. The calculated structural parameters by the DFT method closely match with single crystal XRD data. MEP plays an important role in determining the stability of the molecule. The energies for the various possible conformers of the title compound was calculated and the minimum energy structure was chosen for the computational study as well as for Docking. From the Molecular docking studies, it shows that the positive potential isosurface of MPET are very active and also interact with protein target. Hence this MPET based new compound has also tested to estimate its potential against cholesterol biosynthesis.

Acknowledgement

One of the authors, R.R. Saravanan, feels indebted to Prof. S. Garcia-Granda. The authors thank Misrimal Navajee Munoth Jain Engineering College Management, Thoraipakkam, Chennai 600 097, India for their support. We thank financial support from Spanish Ministerio de Economía y Competitividad (MAT2010-15094, Factoría de Cristalización – Consolider Ingenio 2010, FEDER funds.

Appendix A. Supplementary material

Full crystallographic data for the structural analysis have been deposited with the Cambridge Crystallographic Data Center, CCDC No. 988294. This data can be obtained free of charge via www.ccdc.cam.ac.uk or from Cambridge Crystallographic Data Center, 12 Union Road, Cambridge, CB2, 1EZ, UK (fax: +44 (0)1223 336033 or email: deposit@ccdc.cam.ac.uk).

References

[1] E.M. Bavin, R.J.W. Rees, J.M. Robson, M. Seiler, D.E. Seymour, D. Suddaby, J. Pharm. Pharmacol. 2 (1950) 764–772.
[2] O. Koch, G. Stuttgen, Naunyn Schmiedebergs Arch. Exp. Pathol. Pharmakol. 210 (1950) 409–423.
[3] V. Mishra, S.N. Pandeya, C. Pannecouque, M. Witvrouw, E. De Clercq, Arch. Pharm. (Weinheim) 335 (2002) 183–186.
[4] R.C. Condit, R. Easterly, R.F. Pacha, Z. Fathi, R.J. Meis, Virology 185 (1991) 857–861.
[5] R.A. Finch, M.C. Liu, A.H. Cory, J.G. Cory, A.C. Sartorelli, Adv. Enzyme Regul. 39 (1999) 3–12.
[6] D.L. Klayman, J.F. Bartosevich, T.S. Griffin, C.J. Mason, J.P. Scovill, J. Med. Chem. 22 (1979) 855–862.
[7] H.R. Wilson, G.R. Revankar, R.L. Tolman, J. Med. Chem. 17 (1974) 760–761.
[8] X. Du, C. Guo, E. Hansell, P.S. Doyle, C.R. Caffrey, T.P. Holler, J.H. McKerrow, F.E. Cohen, J. Med. Chem. 45 (2002) 2695–2707.
[9] R.W. Brockman, J.R. Thomson, M.J. Bell, H.E. Skipper, Cancer Res. 16 (1956) 167–170.
[10] J. Easmon, G. Purstinger, G. Heinisch, T. Roth, H.H. Fiebig, W. Holzer, W. Jager, M. Jenny, J. Hofmann, J. Med. Chem. 44 (2001) 2164–2171.
[11] V. Balachandran, K. Parimala, Spectrochim. Acta Part A Mol. Biomol. Spectrosc. 95 (2012) 354–368.
[12] Oxford Diffraction. CrysAlis PRO, CrysAlis CCD and CrysAlis RED. Oxford Diffraction Ltd., Yarnton, Oxfordshire, (2010) England.
[13] M.C. Burla, R. Caliandro, M. Camalli, B. Carrozzini, G.L. Cascarano, L. De Caro, C. Giacovazzo, G. Polidori, D. Siliqi, R. Spagna, J. Appl. Crystallogr. 40 (2007) 609.
[14] G.M. Sheldrick, Acta Crystallogr. A 64 (2008) 112.
[15] L.J. Farrugia, J. Appl. Cryst. 30 (1997) 565.
[16] C.F. Macrae, I.J. Bruno, J.A. Chisholm, P.R. Edgington, P. McCabe, E. Pidcock, L. Rodriguez-Monge, R. Taylor, J. van de Streek, P.A. Wood, J. Appl. Crystallogr. 41 (2008) 466.
[17] L.J. Farrugia, J. Appl. Crystallogr. 32 (1999) 837.
[18] A.L. Speck, J. Appl. Crystallogr. 36 (2003) 7.
[19] M. Nardelli, J. Appl. Crystallogr. 28 (1995) 659.
[20] R. John Xavier, E. Gopinath, Spectrochim. Acta A 97 (2012) 215.
[21] M.J. Frisch, G.W. Trucks, H.B. Schlegel, G.E. Scuseria, M.A. Robb, J.R. Cheeseman, J.A. Montgomery, T.Jr. Vreven, K.N. Kudin, J.C. Burant, J.M. Millam, S.S. Iyengar, J. Tomasi, V. Barone, B. Mennucci, M. Cossi, G. Scalmani, N. Rega, G.A. Petersson, H. Nakatsuji, M. Hada, M. Ehara, K. Toyota, R. Fukuda, J. Hasegawa, M. Ishida, T. Nakajima, Y. Honda, O. Kitao, H. Nakai, M. Klene, X. Knox, J.E. Li, H.P. Hratchian, J.B. Cross, V. Bakken, C. Adamo, J. Jaramillo, R. Gomperts, R.E. Stratmann, O. Yazyev, A.J. Austin, R. Cammi, C. Pomelli, J.W. Ochterski, P.Y. Ayala, K. Morokuma, G.A. Voth, P. Salvador, J.J. Dannenberg, V.G. Zakrzewski, S. Dapprich, A.D. Daniels, M.C. Strain, O. Farkas, D.K. Malick, A.D. Rabuck, K. Raghavachari, J.B. Foresman, J.V. Ortiz, Q. Cui, A.G. Baboul, S. Clifford, J. Cioslowski, B.B. Stefanov, G. Liu, A. Liashenko, P. Piskorz, I. Komaromi, R.L. Martin, D.J. Fox, T. Keith, M.A. Al-Laham, C.Y. Peng, A. Nanayakkara, M. Challacombe, P.M.W. Gill, B. Johnson, W. Chen, M.W. Wong, C. Gonzalez, J.A. Pople, Gaussian, Inc., Wallingford, CT. (2004).
[22] H.B. Schlegel, J. Comput. Chem. 3 (1982) 214.
[23] P. Hohenberg, W. Kohn, Phys. Rev. B 136 (1964) 864–871.
[24] D.J. Becke, Chem. Phys. 98 (1993) 5648.
[25] C. Lee, W. Yang, R.G. Parr, Phys. Rev. B 37 (1988) 785.
[26] A. Frisch, A.B. Neilson, A.J. HolHolder, Gaussview User Manual Gaussian: Pittsburgh. (2000).
[27] G. Wang, F. Jian, Y.F. Ding, Acta Crystallogr. E 64 (2008) o1730.
[28] I. Fleming, Frontier Orbitals and Organic Chemical Reactions, John Wiley and Sons, New York, 1976.
[29] J.S. Murray, K. Sen, Molecular Electrostatic Potentials, Concepts and Applications, Elsevier, Amsterdam, 1996.
[30] J.M. Seminario, Recent Developments and Applications of Modern Density Functional Theory, Elsevier 4 (1996) 800–806.
[31] T. Yesilkaynak, G. Binzet, F. Mehmet Emen, U. Florke, N. Kulcu, H. Arslan, Eur. J. Chem. 1 (2010) 1.
[32] R.R. Saravanan, S. Seshadri, S. Gunasekaran, R. Mendoza-Meroño, S. Garcia-Granda, Spectrochim. Acta Part A Mol. Biomol. Spectrosc. 121 (2014) 268–275.
[33] S. Gunasekaran, U. Ponnambalam, S. Muthu, S. Ponnusamy, Asian J. Chem. 16 (2004) 1513–1518.
[34] J. Fulara, M.J. Nowak, L. Lapinski, A. Les, L. Adamowicz, Spectrochim. Acta Part A Mol. Biomol. Spectrosc. 47 (1991) 595–613.
[35] R.G. Parr, R.G. Pearson, Am. J. Chem. Soc. 105 (1983) 7512–7516.
[36] G. Socrates, Infrared and Raman Characteristic Group Frequencies-Tables and Charts, third ed., Wiley, New York, 2001.
[37] L.J. Bellamy, The Infrared Spectra of Complex Molecule, third ed., Willey, New York, 1975.
[38] L. Clougherty, J. Sousa, G. Wyman, J. Org. Chem. 22 (1957) 462.
[39] R. Kubler, R.W. Luttke, S. Weckherlin, Z. Elektrochem. 64 (1960) 650.
[40] K.J. Morgan, J. Chem. Soc. (1961) 2151–2159.
[41] L.G. Crane, D. Wang, L.M. Sears, B. Heynz, K. Carron, Anal. Chem. 67 (1995) 360.
[42] E.B. Seena, N. Mathew, M. Kuriakose, M.R.P. Kurup, Polyhedron 27 (2008) 1455–1462.
[43] M.F. Sanner, J. Mol. Graph. Model. 17 (1) (1999) 57–61.
[44] K. Stierand, M. Rarey, ChemMedChem 2 (2007) 853.
[45] K. Stierand, P. Maass, M. Rarey, Bioinformatics 22 (2006) 1710–1716.
[46] P.C. Fricker, M. Gastreich, M. Rarey, J. Chem. Inf. Comput. Sci. 44 (3) (2004) 1065.